J Solid State Electrochem (2009) 13:1367–1379
DOI 10.1007/s10008-008-0691-3

ORIGINAL PAPER

Electrochemistry at cobalt(II)tetrasulfophthalocyanine-multi-walled carbon nanotubes modified glassy carbon electrode: a sensing platform for efficient suppression of ascorbic acid in the presence of epinephrine

Bolade O. Agboola · Sibulelo L. Vilakazi · Kenneth I. Ozoemena

Received: 5 July 2008 / Revised: 29 August 2008 / Accepted: 26 September 2008 / Published online: 21 October 2008

Abstract Electrochemistry of water-soluble cobalt(II) tetrasulfophthalocyanine (CoTSPc) electrodeposited on glassy carbon nanotube pre-modified with acid-functionalized multi-walled carbon nanotubes (MWCNT) is described. Both charge transfer resistances toward $[Fe(CN)_6]^{3-/4-}$ redox probe and electrocatalytic responses toward epinephrine (EP) detection follow the trend: bare GCE<GCE-MWCNT<GCE-CoTSPc<GCE-MWCNT-CoTSPc. EP analysis was then carried out in details using GCE-MWCNT-CoTSPc. The catalytic rate constant value $k_{ch}=2.2\times10^7$ (mol $cm^{-3})^{-1}$ s^{-1} was obtained from rotating disk electrode experiment. Interestingly, GCE-MWCNT-CoTSPc efficiently suppressed the detection of ascorbic acid (the natural interference of neurotransmitters in physiological conditions) showing good sensitivity (0.132 ± 0.003 A l mol^{-1}), limit of detection (4.517×10^{-7} mol l^{-1}), and quantification (15.056×10^{-7} mol l^{-1}). In addition, GCE-MWCNT-CoTSPc was conveniently used to determine EP in epinephrine hydrochloric acid injection with recovery of $101.1\pm2.2\%$.

Keywords Epinephrine · Carbon nanotubes · Ascorbic acid

B. O. Agboola · K. I. Ozoemena (✉)
Molecular and Nanomaterials Electrochemistry Laboratory,
Department of Chemistry, University of Pretoria,
Pretoria 0002, South Africa
e-mail: kenneth.ozoemena@up.ac.za

S. L. Vilakazi
Department of Chemistry, University of Limpopo,
Turfloop Campus, Private Bag x 1106, Sovenga, Limpopo 0727,
South Africa

Introduction

Since the re-discovery of carbon nanotubes (CNTs) in 1991 [1], both single-walled (SWCNTs) and multi-walled (MWCNTs) have continued to prove their ideality for constructing efficient electrochemical sensors [2–6]. CNTs also have the ability to interact with organic aromatic compounds through *p–p* electronic and hydrophobic interactions to form new structures because of their rolled-up graphene sheets of carbon, which exhibit a *p*-conjugative structure with a highly hydrophobic surface [7]. On the other hand, redox-active transition metallophthalocyanine (MPc) complexes especially the first transition ones, mainly Fe, Co, Mn, and Ni, have over the years proved to be excellent in electrocatalysis and sensing applications [8–10]. MPc complexes have been used to modify electrodes by different methods, but electropolymerization forms multilayered polymer coatings of the complexes forming a three-dimensional reaction zone at the electrode surface, thus improving the response sensitivity of the electrode [11]. The integration of these two redox-active species as electrode modifiers in heterogeneous electrocatalysis and sensing devices is still very few [12–16]. Recent reports have shown that CNT-MPc hybrids exhibited enhanced electrochemical responses in comparison to the use of CNT or MPc alone. Work on use of these hybrids include the detection of important molecules such as asulam [12], hydrolysis products of V-type nerve agents [13–15], mercaptoethanol, and nitric oxide [16]. Although some work on the use of various substances as electrode modifiers toward epinephrine (EP) electro-oxidation have been reported [17–24], our group reported for the first time on the use of CNT-MPc hybrids specifically self-assembled films of SWCNT and SWCNT integrated to cobalt(II)tetra-aminophthalocyanine (SWCNT-CoTAPc) on gold electrode toward EP electro-oxidation [25]; however,

relatively low sensitivity (9.4×10^{-3} A l mol^{-1}) and high limit of detection (LoD) (6 μmol l^{-1}) were obtained. In this work, we aim at improving on these analytical parameters. Epinephrine exists in the central nervous system (CNS) and body fluid as organic cations. It belongs to the group of catecholamine neurotransmitters found in the mammalian CNS ensuring proper functioning of central nervous, renal, hormonal, and cardiovascular systems. In addition, epinephrine can also be used as drugs for the treatment of disease like hypertension [26]. EP always coexists with ascorbic acid in biological systems mainly in fluids such as blood and urine [27], and therefore, it is not surprising that the major challenge in EP analysis is the elimination of interferences from ascorbic acid (AA). AA oxidation peak is very close to that of EP, which often results to peaks overlapping. Negatively charged nafion ionomer has been used to modify electrodes in order to repel AA from the electrode surface, but low sensitivity was reported for this electrode [28].

In this work, we explored the synergistic effect of combining cobalt tetrasulfophthalocyanine (CoTSPc) and MWCNT toward epinephrine oxidation. The MWCNT, a good electrical conductor, was used as the base material in which CoTSPc was electrochemically deposited (Scheme 1). In addition, the application of this electrode in the sensing and determination of EP in the absence and presence of AA was investigated.

Experimental

Materials and reagents

MWCNTs were obtained from Aldrich, and functionalized MWCNTs were synthesized using established method [29]. In brief, the MWCNTs were functionalized; first, MWCNTs were purified by refluxing in concentrated nitric acid (2.6 mol l^{-1} HNO_3) and then ultrasonicated in a mixture of H_2SO_4 and HNO_3 (3:1, *v*/*v*) and suspended in a mixture of H_2SO_4 and 30% H_2O_2 in order to functionalize it with COOH groups. CoTSPc was synthesized following the well-established Weber and Busch strategy [30]. *N*,*N*-Dimethylformamide (DMF) was purchased from Sigma-Aldrich and was distilled and dried before use. Potassium ferrocyanide ($K_4Fe(CN)_6.3H_2O$) was obtained from B. Jones Ltd., SA; potassium ferricyanide $K_3Fe(CN)_6$ was purchased from Bio-Zone Chemicals, SA. Epinephrine (4-[1-hydroxy-2-(methylamino)ethyl]-1,2-benzenediol) was obtained from Sigma-Aldrich. Ultrapure water of resistivity 18.2 MΩ cm was obtained from a Milli-Q Water System (Millipore, Bedford, MA, USA) and was used throughout for the preparation of solutions. Phosphate buffers were prepared using appropriate amounts of H_3PO_4, KH_2PO_4, K_2HPO_4, and K_3PO_4 depending on the pH. All electrochemical experiments were carried out in nitrogen atmosphere. All other reagents were of analytical grade and were used as received from the suppliers without further purification.

Apparatus asnd procedure

Electrochemical studies were carried out using an Autolab potentiostat PGSTAT 302 (Eco Chemie) driven by the General Purpose Electrochemical Systems data processing software (GPES, software version 4.9). The working electrode was bare glassy carbon electrode (GCE, BASi, South Africa, 3.0 mm diameter) or the same GCE modified. Ag|AgCl sat'd KCl reference and platinum wire counter electrodes were employed. Electrochemical impedance spectroscopy (EIS)

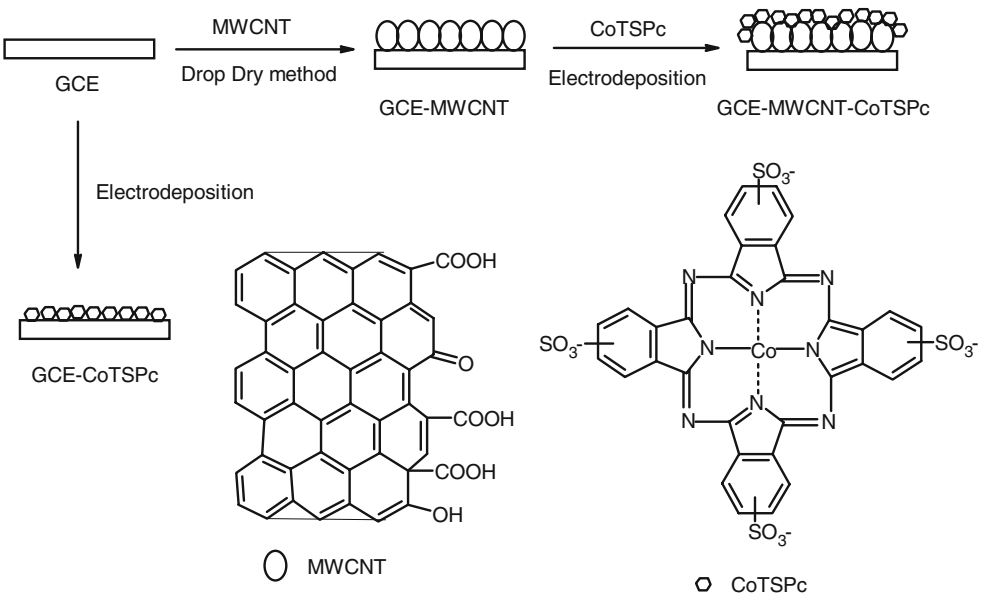

Scheme 1 Schematic representation of synthetic route for electrodes fabrication

measurements were performed with Autolab FRA software between 1.0 Hz and 10 kHz using a 5 mV rms sinusoidal modulation. pH measurements were performed using Labotec Orion bench top pH meter model 420A. The RDE experiments were performed using Autolab-RDE (Eco Chemie, Utrecht, The Netherlands), with a RDE glassy carbon tip (5.0 mm in diameter) as the working electrode. All experiments were performed at room temperature. Solutions were deaerated by bubbling nitrogen prior to the experiments, and the electrochemical cells were kept under a nitrogen atmosphere throughout the experiments. The electrode fabricated is summarized as shown in Scheme 1.

Prior to electrode modification, the bare GCE (both glassy carbon electrodes and plates) was first cleaned by polishing with aqueous slurry of alumina, rinsing with distilled water, sonicated in ethanol, and finally cleaned with tissue paper. The electrode was then modified with MWCNT using the drop-dry technique. The drop-dry procedure involved placing a drop of MWCNT in DMF solution (1 mg ml^{-1}). In order to ensure that the procedure is reproducible, evenly spread one drop (1 μl) of the MWCNT in DMF solution was put on the surface of the GCE. The electrode was then put in the oven to dry at 50 °C for 2 min and allowing cooling to room temperature. Electrodeposition of CoTSPc complex on glassy carbon electrode with MWCNT layer was performed by repetitive scanning (CV) of the complex solution (1 mM) in DMF containing tetrabutylammonium tetrafluoroborate ($TBABF_4$) at the potential window from +1.2 and −1.2 V versus Ag|AgCl at a scan rate of 100 mV s^{-1}. The modified electrodes were stored in phosphate buffer solutions (pH 7.0) and rinsed in the same solution prior to use. All the AFM experiments were performed with AFM 5100 System (Agilent Technologies, USA) using a contact mode AFM scanner interfaced with a PicoView 1.4.3 controller (scan range, 1.25 μm in *x*–*y* and 2.322 μm in *z*). Silicon type PPP-CONT-20 (Nanosensors®) of thickness 2.0±1.0, length 450±10, width 50±7.5 μm, spring constants 0.02–0.77 N m^{-1}, resonant frequencies of 6–21 kHz, and tip height of 10–15 μm were used. All images (256 samples/line×256 lines) were taken in air at room temperature and at scan rates 0.5–0.6 lines s^{-1}.

Results and discussion

AFM characterization of electrodes

Figure 1 shows AFM images of the electrodes investigated in this work. Judging from the topographies and cross-sections, the glassy carbon plate (GCP, Fig. 1a) depicts a fairly smooth surface. On electrodeposition of CoTSPc, island-like clusters due to aggregation of CoTSPc molecules were observed (Fig. 1b). Figure 1c shows the AFM topography image for MWCNT modified glassy carbon electrode, where aggregated cluster-like structures of the CNTs can be observed. The CoTSPc-MWCNT (Fig. 1d) shows a more compact image possibly due to the π–π interaction between the two species.

Voltammetric and impedimetric characterization of electrodes

Figure 2a–d respectively show the CVs obtained at (a) bare GCE, (b) GCE-MWCNT, (c) GCE-CoTSPc, and (d) GCE-MWCNT-CoTSPc in 0.5 mol l^{-1} H_2SO_4.

No peak was observed for the CV obtained at the bare GCE (Fig. 2a), but the CVs obtained at other electrodes showed broad quasi reversible peaks each; this is an indication that the GC electrode has been modified with redox active species. From Fig. 2b (GCE-MWCNT), no clear redox peaks was observed, while redox couples at $E_{1/2}$ $(E_{pa}+E_{pc})/2 \approx 0.25$ V and $E_{1/2}$ $(E_{pa}+E_{pc})/2 \approx 0.45$ V (vs. Ag|AgCl, sat'd KCl) at GCE-CoTSPc (Fig. 2c) and GCE-MWCNT-CoTSPc (Fig. 2d), respectively, were observed. These redox couples are characteristic signatures of the respective central metal redox activity ($Co^{III}Pc^{-2}/Co^{II}Pc^{-2}$) [31, 32]. The positive shift in the redox peak as seen in Fig. 2d for GCE-MWCNT-CoTSPc electrode compared to Fig. 2c for GCE-CoTSPc electrode could be due to the presence of MWCNT in the former. The surface concentrations of the redox active species (MWCNT and CoTSPc) were estimated from the anodic peaks (CV experiments) as shown in Fig. 2c and d. Essentially, only the CoTSPc showed active redox peaks at these potential range as judged from the insignificant appearance of peaks at the GCE-MWCNT (Fig. 2b). The surface concentrations (Γ mol cm^{-2}) were determined from the area (charge, Q) under the anodic peaks using the following relationship [9, 10] (Eq. 1):

$$\Gamma = \frac{Q}{nFA} \tag{1}$$

where n represents number of electrons transferred (≈ 1), F is the Faraday constant (9,6485 °C mol^{-1}), and A is the estimated actual surface area of the electrode (≈0.07 cm^2). The surface concentrations were calculated, respectively, for CoTSPc at CoTSPc-GCE (Fig. 1c) and MWCNT/CoTSPc-GCE electrodes (Fig. 1d) as 3.20×10^{-10} and 6.55×10^{-10} mol cm^{-2} respectively. The much higher surface concentration of CoTSPc on the GCE-MWCNT-CoTSPc (~2 folds) compared to the CoTSPc-GCE electrode can be due to the possible different arrangements of the CoTSPc on bare electrode and on MWCNT base GCE electrode. A thin film of the MWCNT base should allow a

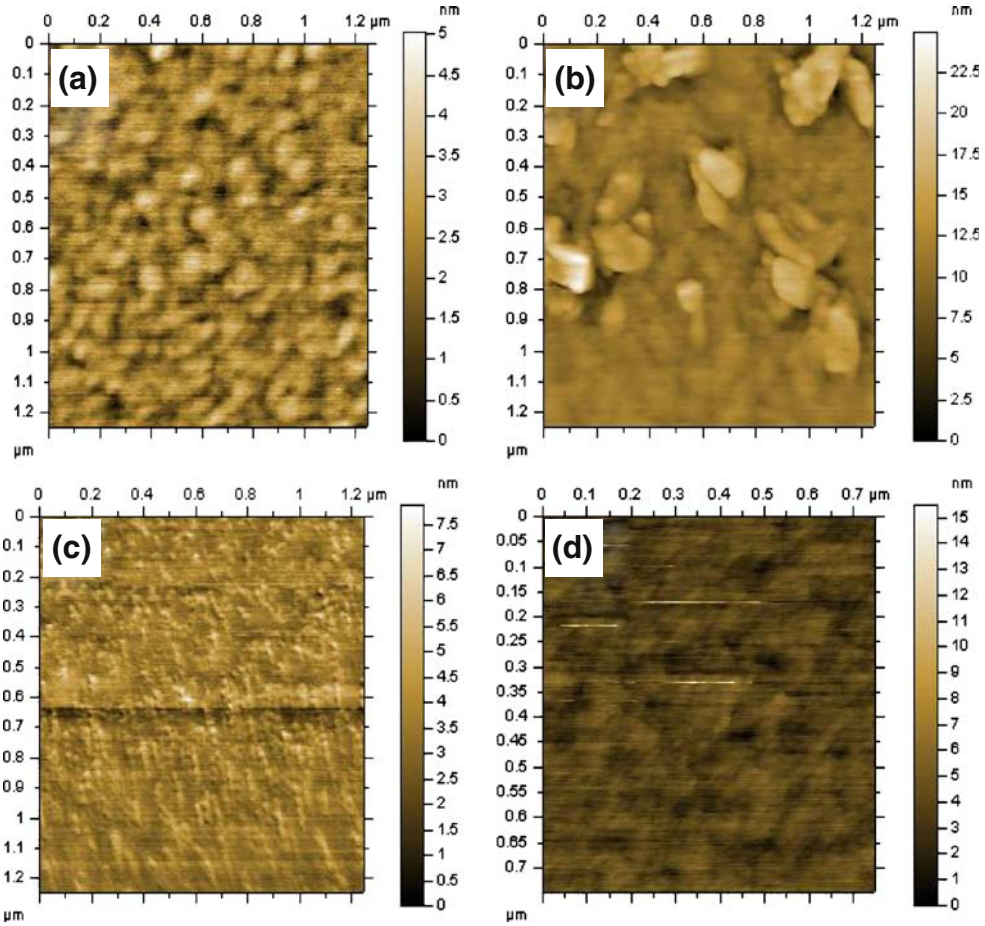

Fig. 1 Contact-mode AFM images of **a** bare glassy carbon plate (GCP), **b** GCP-MWCNT, **c** GCP-CoTSPc, and **d** GCP-MWCNT-CoTSPc

more attachment of the CoTSPc due to more surface area created by the morphology of the MWCNT on the GCE electrode; MWCNT are tubular in nature and so the electrode surface will be relatively rough.

Figure 3 shows the CVs response of these electrodes in 1 mmol l^{-1} $[Fe(CN)_6]^{4-}/[Fe(CN)_6]^{3-}$ in 1 mol l^{-1} KCl.

Decrease in the ΔE values were observed upon modification; thus, the presence of the modifiers increased the rate of electron transfer for the $[Fe(CN)_6]^{4-}/[Fe(CN)_6]^{3-}$ oxidation. Enhanced I_p were observed for these electrodes relative to the bare GCE in this order: GCE-MWCNT-CoTSPc (19.0 μA)>GCE-CoTSPc (16.9 μA)>GCE-MWCNT (15.7 μA) > bare GCE (10.6 μA), indicating more catalytic sites at the surface of these electrodes in the above order. EIS was employed to give insights into the charge transfer kinetics occurring at these electrodes. EIS is a powerful non-destructive and very informative technique for probing molecules at surfaces. It provides vital information about processes at the electrode|electrolyte interface [33–35]. Figure 4 shows the Nyquist plots obtained for the electrodes in $[Fe(CN)_6]^{4-}/[Fe(CN)_6]^{3-}$ solution.

The experimental data were fitted with the modified Randles equivalent circuit (Fig. 5a) involving constant phase element (CPE) rather than the ideal double layer capacitance (C_{dl}) for bare GCE, GCE-CoTSPc, and GCE-MWCNT electrodes while the circuit (Fig. 5b) respectively fitted for GCE-MWCNT-CoTSPc electrode.

In these circuits, R_s represents that solution resistance, R_{ct} is the electron-transfer resistance (domain of kinetic control), and Z_w is the Warburg impedance (domain of mass transport control) resulting from the diffusion of ions to and from the electrode|solution interface. CPE model for simulating EIS data incorporates the non-homogeneity (roughness) of the electrode surfaces; that is, the CPE is due to the energetic inhomogeneity of the electrodes [34, 35]. The incorporation of CPE element gives better fittings for pseudocapacitive systems. The impedance of the CPE (Z_{CPE}) is a power-law-dependent interfacial capacity given as shown in Eq. 2:

$$Z_{CPE} = [Q(j\omega)^n]^{-1} \quad (2)$$

where Q is the frequency-independent constant, ω is the radial frequency, and n is a factor describing the deviation from the ideal capacitive behavior. An n value of 0

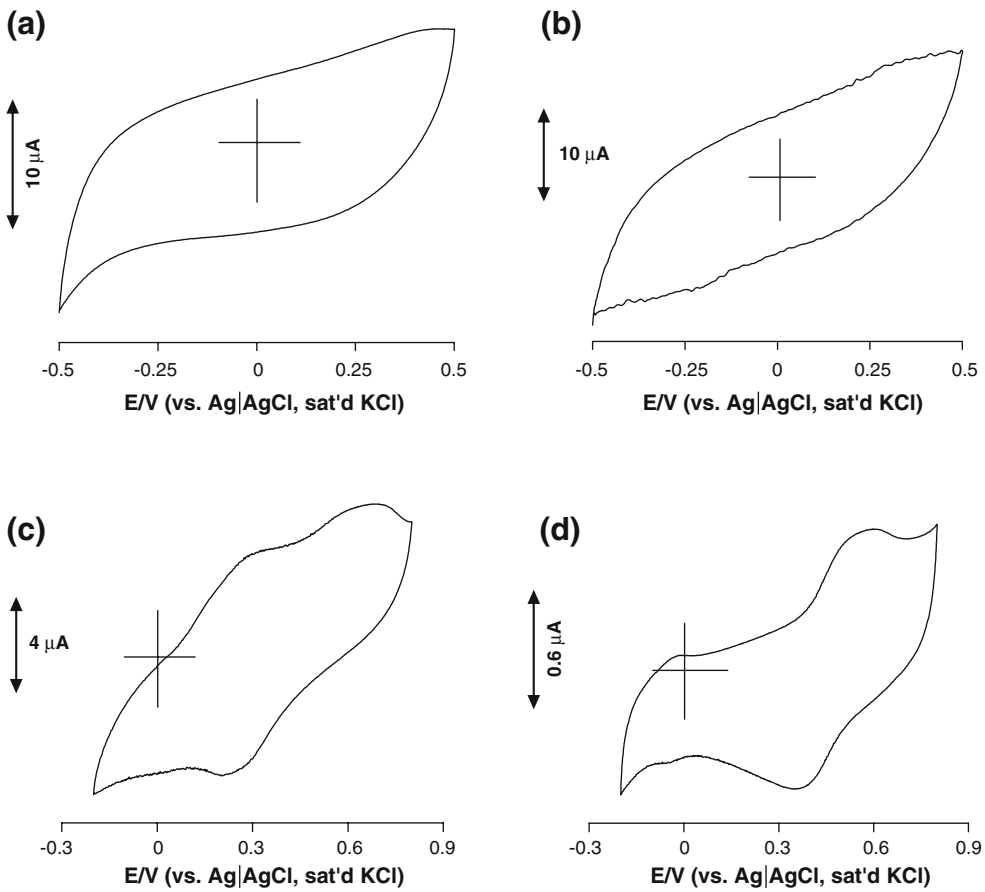

Fig. 2 Typical cyclic voltammograms obtained at **a** bare GCE, **b** GCE-MWCNT, **c** GCE-CoTSPc, and **d** GCE-MWCNT-CoTSPc in 0.5 mol l^{-1} H_2SO_4. Scan rate=50 mV s^{-1}

corresponds to a pure resistor; a unit value of *n* corresponds to a pure capacitor, while a 0.5 value corresponds to Warburg impedance. The difference in the fittings from one electrode to the other can be ascribed to the different chemical nature of the electrode modifier resulting to different kinetics and mechanisms of electron transfer at the surface of the electrodes. It was observed that the order of the R_{ct} is as follows: GCE-MWCNT-CoTSPc (0.32 KΩ) > GCE-MWCNT (3.41 KΩ) > GCE-CoTSPc (5.31 KΩ) ≈ bare GCE (5.15 KΩ). The fact that the R_{ct} value for the GCE-MWCNT-CoTSPc is significantly smaller than the other electrodes is an indication that the combination of MWCNT and CoTSPc is synergic toward enhancement of $Fe(CN)_6]^{-3/-4}$ redox process. From Table 1, *n* values extracted from the fitted Nyquist plots for all the electrodes suggest deviation from ideal capacitive behavior. All the fitted values shown in Table 1 were obtained after several iterations. Bode plots [i.e., log |*Z*| (Fig. 6a) and −phase angle (Fig. 6b) vs. log *f*] validate the conclusions from Nyquist plot fittings.

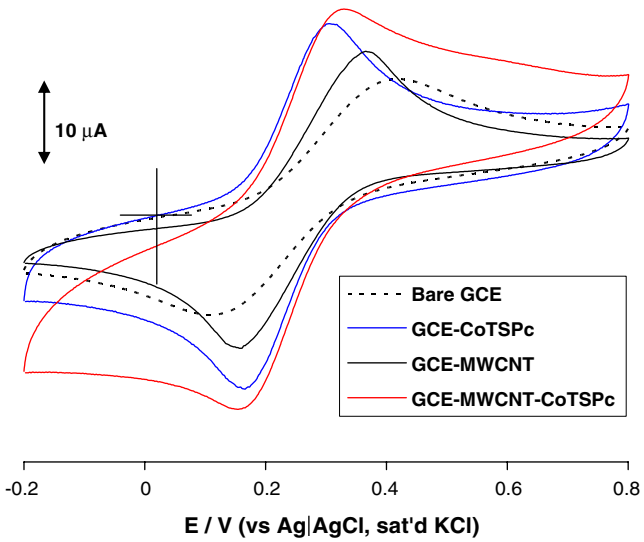

Fig. 3 Cyclic voltammograms obtained at the electrodes in 1 mmol l^{-1} $Fe(CN)_6^{3-/4-}$ in 0.1 mol l^{-1} KCl. Scan rate=50 mV s^{-1}

The values of the slope at low and high frequency regions for the respective electrodes are bare GCE (−0.132, −0.046), GCE-MWCNT (−0.38, −0.036), GCE-CoTSPc (−0.365, −0.057), GCE-MWCNT-CoTSPc (−0.262, −0.058); these values are far from the value of −0.1 indicating that these electrodes exhibit pseudo-capacitive behavior. This further corroborates the incorporation of the CPE element in the equivalent circuit. The electrodes exhibited capacitive relaxation at different phase angles and frequency from one to

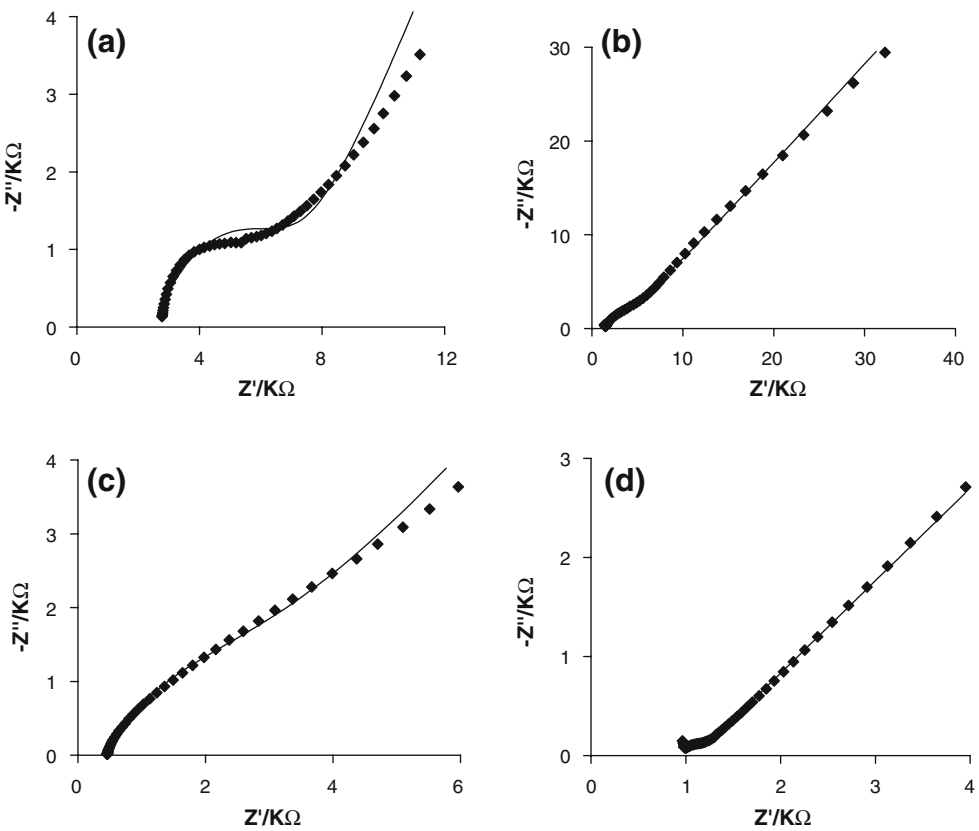

Fig. 4 Nyquist plots obtained in $Fe(CN)_6^{3-/4-}$ 0.1 mol l^{-1} KCl at **a** bare GCE, **b** GCE-MWCNT, **c** GCE-CoTSPc, and **d** GCE-MWCNT-CoTSPc. Applied potential=$E_{1/2}$ (V) (vs. Ag|AgCl, sat'd KCl)

another, an indication of different charge transfer kinetics at the solution-electrode interface from one electrode to the other. The values are as follows: bare GCE (~15.15° at 2.37 Hz), GCE-MWCNT (~36.25° at 0.94 Hz), GCE-CoTSPc (~40.63°, 28.86° at -0.29, 1.86 Hz), and GCE-MWCNT-CoTSPc (~5.94° at 2.57 Hz). The phase angle values for all the electrodes are all less than 90°, thus confirming the pseudo-capacitive behavior of the electrodes. Furthermore, the shift in the phase angle frequencies of the modified electrodes compared to the bare GCE is an indication that the reactions are now occurring at the modifiers and not at bare GCE electrode surface.

Electrochemical studies of epinephrine oxidation: comparative cyclic voltammetric analysis

Figure 7 shows the CVs of 10^{-4} mol l^{-1} EP in phosphate buffer solution pH 7.4 at bare GCE (curve a), GCE-MWCNT (curve b), GCE-CoTSPc (curve c), and GCE-CoTSPc/MWCNT (curve d).

From Fig. 7a to d, the EP electro-oxidation is irreversible; it is the oxidation of epinephrine to epinephrinequinone via removal of the two protons of the enol end of epinephrine (Eq. 3). This is the mechanism established for EP oxidation on CNT modified electrodes [2, 36].

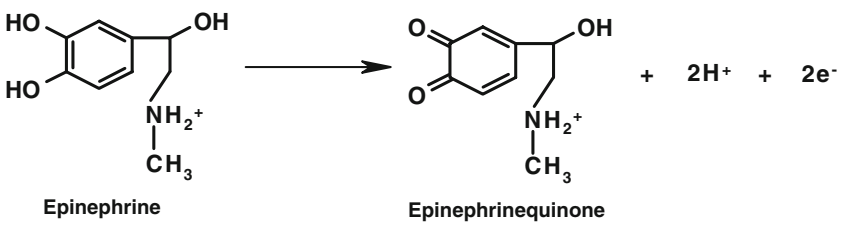

(3)

EP oxidation obtained at the GCE-MWCNT-CoTSPc showed the best catalysis compared to the rest in terms of peak current, I_p. It can be observed from Fig. 7 that the E_p position for EP electro-oxidation at GCE-MWCNT occurred at a lower positive potential compared to that of GCE-MWCNT-CoTSPc, a similar observation [16] in

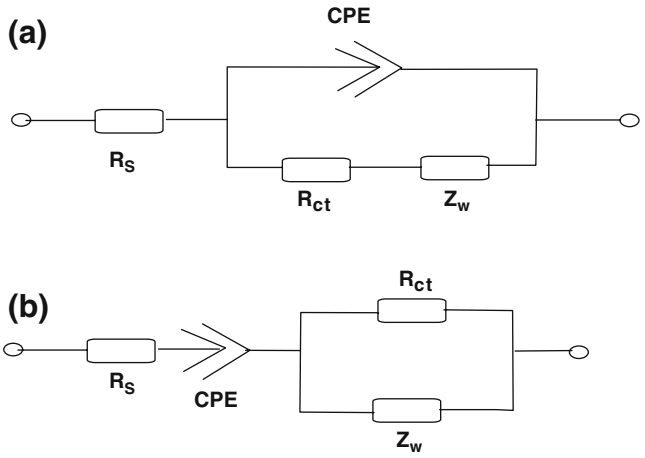

Fig. 5 Equivalent circuits for 1 mmol l^{-1} $Fe(CN)_6^{3-/4-}$ in 0.1 mol l^{-1} KCl at the electrode **a** bare GCE, GCE-MWCNT, and GCE-CoTSPc and **b** GCE-MWCNT-CoTSPc. Applied potential=$E_{1/2}$ (V) (vs. Ag|AgCl, sat'd KCl)

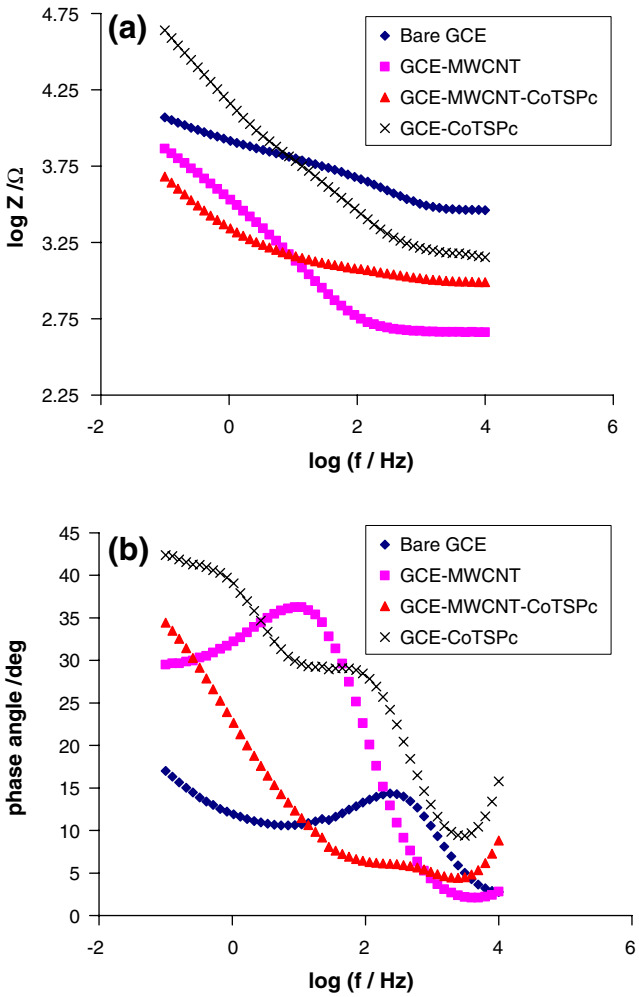

Fig. 6 Bode plots **a** log Z versus log f and **b** −phase angle versus log f in $Fe(CN)_6^{3-/4-}$ 0.1 mol l^{-1} KCl solution at various electrodes. Applied potential=$E_{1/2}$ (V) (vs. Ag|AgCl, sat'd KCl)

which the nitric oxide (NO) electro-oxidation E_p occurred at a lower positive potential at GC-SWCNT compare to that of GC-SWCNT-NiTSPc was reported. The authors associated this observation to the different electrocatalytic features on both SWCNT and NiTSPc; in our own case, MWCNT and CoTSPc are also expected to exhibit different electrocatalytic features. Furthermore, the enhanced I_p current observed at GC-SWCNT-NiTSPc, which is favorable for analytical purposes, could be explained by the fact that MWCNT provided a higher surface area for CoTSPc deposition and at the same time a good electrical nanowires link between CoTSPc and the GCE.

In addition, the improved catalysis at the GCE-MWCNT-CoTSPc may be attributed to the presence of the CoTSPc, being first row transition metal phthalocyanines that are known [37–39] to catalyze several analytes via the central metal ion. Consequently, GCE-MWCNT-CoTSPc was used only for further analysis. The effect of scan rate variation on the CVs of EP oxidation (not shown) shows that peak current (I_p) of the epinephrine oxidation gave good linear relationship with the square root of scan rate ($\nu^{1/2}$) with R^2=0.9988, indicating a diffusion-controlled reaction and a good indication of the electrode analytical applicability.

Chronoamperometric analysis

Figure 8 shows a well-resolved chronoamperometric evolutions obtained at 0.38 V with increasing concentrations of epinephrine (2.44–3.00 μmol l^{-1}) in phosphate buffer solution, pH 7.4.

A linear relationship between transient catalytic current (measured at 5 s) and epinephrine concentrations was obtained as:

Table 1 Summary of impedimetric evolutions of the electrodes

Electrode	R_s/KΩ	R_{ct}/KΩ	10^4 Q/μF	n	$10^3 Z_w$/Ω cm^2
Bare GCE	2.51 (1.95)	5.15 (4.51)	0.10 (14.14)	0.53 (4.18)	0.22 (3.62)
GCE-MWCNT	0.45 (0.71)	3.41 (4.90)	0.38 (5.32)	0.73 (1.37)	0.23 (2.69)
GCE-CoTSPc	1.31 (3.38)	5.31 (32.2)	0.71 (41.82)	0.64 (8.54)	0.25 (11.07)
GCE-MWCNT-CoTSPc	0.76 (5.29)	0.32 (9.88)	3.22 (0.91)	0.48 (1.24)	1.46 (31.27)

Percentage errors are in brackets

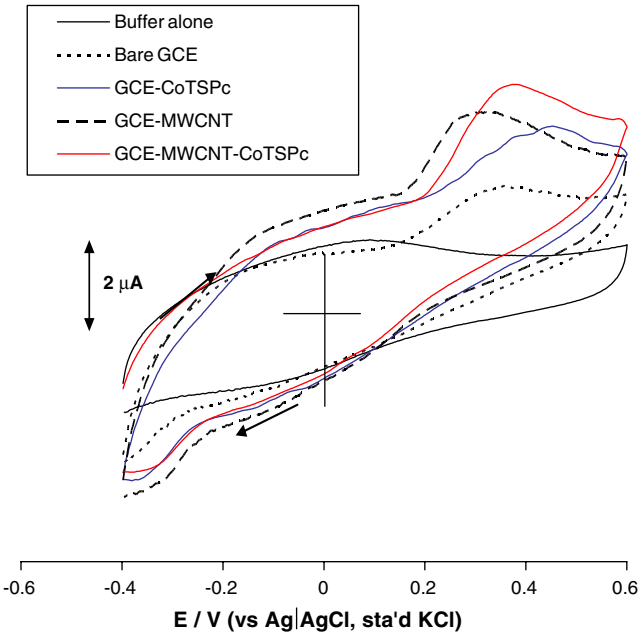

Fig. 7 Cyclic voltammograms obtained for (1) phosphate buffer pH 7.4 alone and (2) 10^{-4} mol l^{-1} EP electro-oxidation in phosphate buffer pH 7.4 at various electrodes. Scan rate=50 mV s^{-1}

$$I_{cat}/A = (0.132 \pm 0.002)[\text{epinephrine}]/\}\text{mol}\,l^{-1} + (0.40 \pm 0.20)10^{7}\left(R^2 = 0.9957\right) \quad (4)$$

The sensitivity value, 0.132±0.003 A l mol^{-1}, was obtained. LoD=3 δ/m and the limit of quantification (LoQ)=10 δ/m, where δ is the relative standard deviation of the intercept of the y-coordinates from the line of best fit and m the slope of the same line. The LoD was calculated as 4.517×10^{-7} mol l^{-1}. The quantification limit (LoQ) describes the lowest concentration of an analyte that can be quantified with acceptable precision and accuracy, and the value obtained was 15.056×10^{-7} mol l^{-1}.

Rotating disc electrode experiment

Figure 9a shows the RDE voltammograms obtained at different rotating speed (ω) for 10^{-4} mol l^{-1} EP electro-oxidation in phosphate buffer pH 7.4 using GCE-MWCNT-CoTSPc, and Fig. 9b shows the plot of limiting current (I_L) versus $\omega^{1/2}$ (Koutecky–Levich plot).

The Koutecky–Levich plot was found to be linear with positive intercept; this indicates that the electrode reactions are controlled by both kinetics at the electrode surface and the mass transport of epinephrine species at the electrode surfaces. Using Eq. 5 below,

$$\frac{1}{i_{lim}} = \frac{1}{i_k} + \frac{1}{i_{lev}} = \frac{1}{(nFAk_{ch}\Gamma C)} + \frac{1}{\left(0.620nFAcD^{2/3}\gamma^{-1/6}\omega^{1/2}\right)} \quad (5)$$

where i_{lim}, i_k, i_{lev} are the measured current, kinetic, and diffusion-limited currents, respectively, n is the number of electrons transferred which is 2 for EP electrooxidation, k_{ch} is the catalytic rate constant (mol^{-1} cm^3 s^{-1}), F is the Faraday constant (96,485 °C mol^{-1}), A is the electrode surface area which is 0.1963 cm^2, ω is the rotating speed (rps), Γ (mol cm^{-2}) is the redox active species (CoTSPc/MWCNT) concentration on electrode surface, c is the bulk concentration of EP (10^{-7} mol cm^{-3}), D is the diffusion coefficient (cm s^{-1}) of EP, and γ is the kinematic viscosity of the solution.

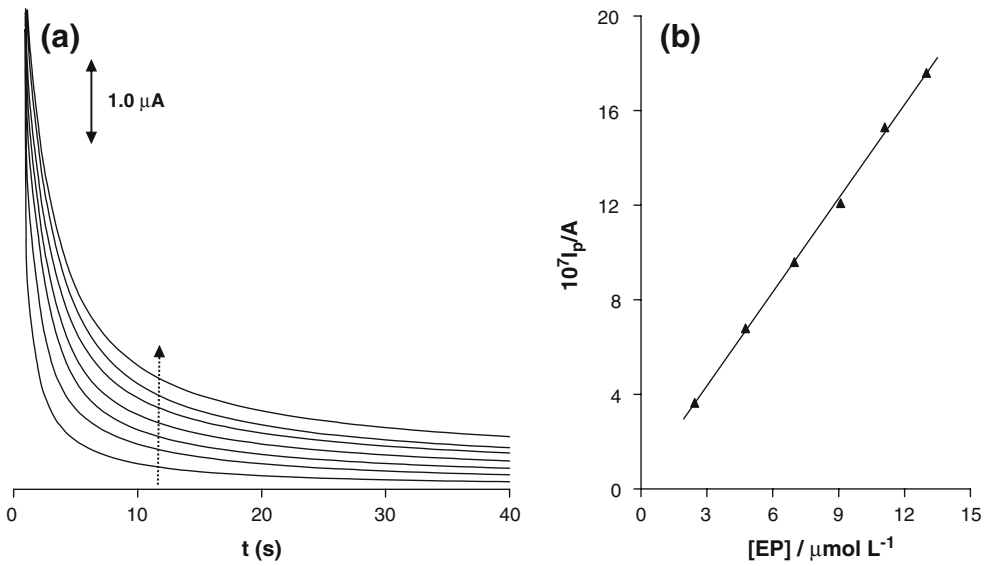

Fig. 8 **a** Chronoamperomograms obtained for EP electro-oxidation concentration studies and plot of **b** I_p versus (EP) in phosphate buffer pH 7.4 using GCE-MWCNT-CoTSPc electrode

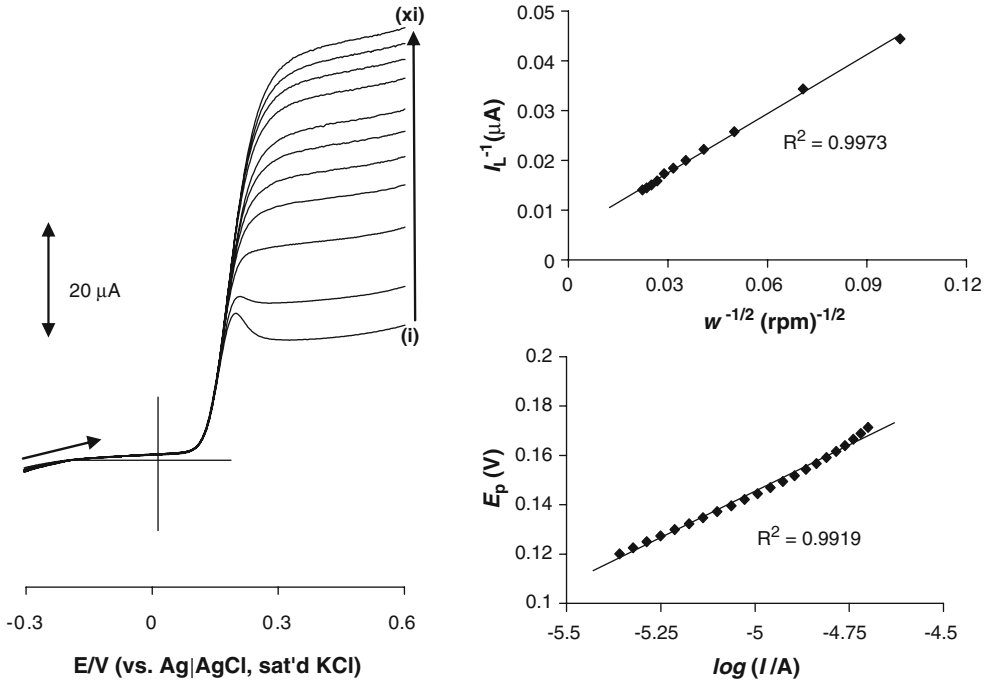

Fig. 9 **a** RDE voltammograms obtained at different rotating speed (ω) for 10^{-4} mol l^{-1} EP electro-oxidation in phosphate buffer pH 7.4 using GCE-MWCNT-CoTSPc, **b** plot of I_p^{-1} versus $\omega^{-1/2}$, and **c** Tafel slope for the oxidation of EP from RDE experiment. Scan rate= 50 mV s^{-1}

$$\mathrm{II}(\mu\mathrm{A}) = (1.404)\omega^{1/2}\left(\mathrm{rad\,min^{-1}}\right)^{1/2} + (9.699)(\mu\mathrm{A})\left(R^2 = 0.9973\right) \quad (6)$$

The k_{ch} value obtained from the intercepts of the regression lines was found to be 2.2×10^7 mol^{-1} cm^3 s^{-1}, in comparison to the k_{ch} value obtained at [Os(bpy)$_2$(PVP)$_{10}$Cl]Cl polymer-based electrode [40], which is in the order of 10^4 for epinephrine. It can be said that there is a faster kinetics between the EP and the electrode surface at the GCE-MWCNT-CoTSPc than at the [Os(bpy)$_2$(PVP)$_{10}$Cl]Cl polymer based electrode.

Tafel plot (Fig. 9c) was plotted from the RDE data; this is the plot of the applied potential vs. the log of the kinetic current. At all the potentials, the slope values are close to 70 mV dec^{-1}. A Tafel slope close to 60 mV dec^{-1} suggests a catalyst fast redox process as the first step followed by a non-redox (chemical step) rate-determining step (rds) such as analyte binding with the catalyst or possible deprotonation of the analyte [41, 42] as a possible mechanism. The catalyst redox process could be the Co^{2+} Pc to Co^{3+} Pc redox processes of the MPc and then followed by rate determining chemical step involving possible pi–pi interaction between Co^{3+} Pc/SWCNT and EP molecule as illustrated in Eq. 7.

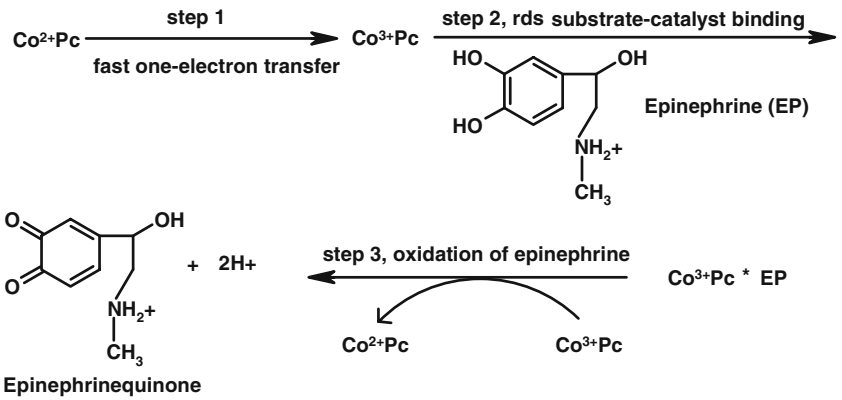

(7)

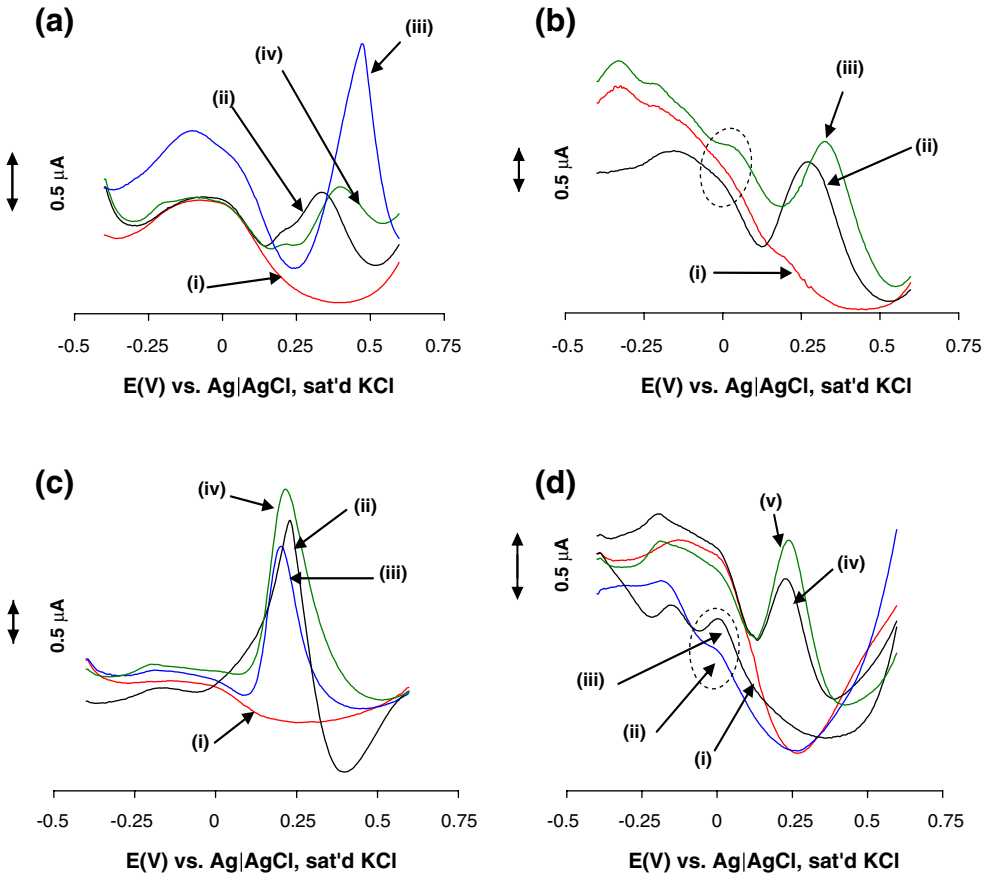

Fig. 10 Square wave voltammograms (SWV) for EP, AA only or their mixtures in phosphate buffer pH 7 obtained at **a** bare GCE, **b** GCE-MWCNT, **c** GCE-CoTSPc, and **d** GCE-MWCNT-CoTSPc

Regeneration, reproducibility, and stability

GCE-MWCNT-CoTSPc electrode was tested for its stability and reproducibility; a decrease in the peak current (~20%) occurred after the first scan, but it was found that the electrode could be regenerated by rinsing it in phosphate buffer solution (pH 7.4) for about a minute. Repetitive scan (ten times) with rinsing in phosphate buffer after every scan showed no significant differences in the peak current (I_p) with scan number (RSD ≈ 4.8%). Furthermore, the electrode was found to be stable even after 2 weeks, showing no significant change in current response.

Interference studies: comparative electrochemical response toward EP in the presence of AA

Ascorbic acid usually coexists with epinephrine in biological system, and therefore, electrochemical determination of both molecules simultaneously is important. At bare electrodes, (GCE, Au etc.), their peaks are not resolved, making it impossible for their determination. The responses of all the electrodes toward EP in the presence of AA were evaluated, as shown in Fig. 10a and b.

At the bare GCE, the 1 µmol l^{-1} EP and 1 mmol l^{-1} AA E_p values appeared respectively at relatively high positive potentials 0.35 and 0.47 V, while a single peak at 0.42 V appeared when the two molecules were determined simultaneously as shown in Fig. 10a. Figure 10b showed the responses obtained for the same solutions using GCE-MWCNT. EP E_p values appeared at 0.28 V. Furthermore, the electrode resolved both EP and AA peaks when they were simultaneously determined, with their E_p values at 0.34 and 0.05 V, respectively. However, a drastic shift in the E_p position for EP from 0.28 to 0.34 V occurred, an indication of AA interference in the determination of EP. At the GCE-CoTSPc electrode (Fig. 10c), the E_p positions for AA, EP, and the mixture of both of them appeared around 0.24 V, a value close to the $E_{1/2}$ for the Co^{2+}/Co^{3+} redox couple of the CoTSPc, indicating that the mechanism for the electro-oxidation of both molecules markedly depended on the Co^{2+}/Co^{3+} redox activity and thus making resolution of their peaks not to be possible. Figure 10d showed the responses obtained at GCE-MWCNT-CoTSPc electrode. The response for the 1 mmol l^{-1} AA appeared at 0.013 V, but clearly defined peak (at the same potential) could only be observed when the concentration of AA was increased from 1 to 2 mmol l^{-1}. Only the EP peak was observed for

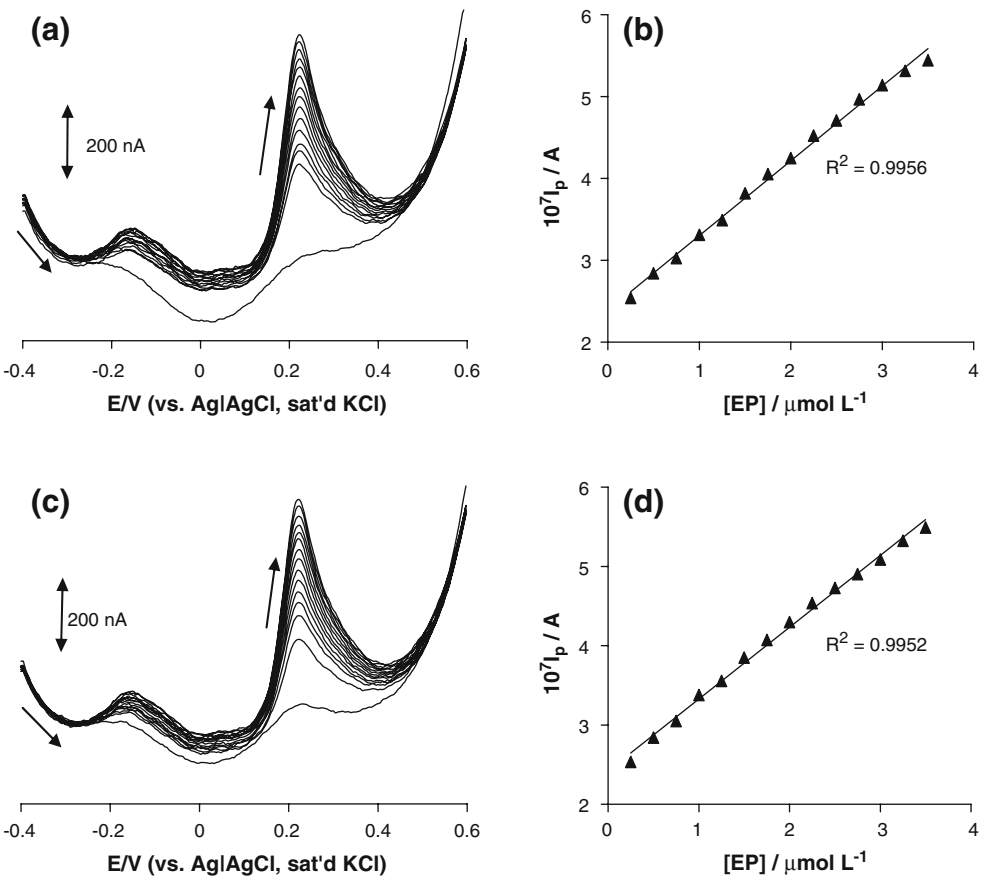

Fig. 11 Square wave voltammograms obtained at different concentrations of EP in (**a**, *i*) phosphate buffer pH 7 and (**a**, *ii*) 10^{-3} mol l^{-1} AA phosphate buffer pH 7, (**b**, *i*) and (**b**, *ii*) are their respective I_p versus (EP) plots

their simultaneous determination, and there was no significant difference in the E_p position (0.01 V) compared to that obtained for 1 μm EP. Consequently, detailed interference studies of AA in EP determination using GCE-MWCNT-CoTSPc electrode was then carried out.

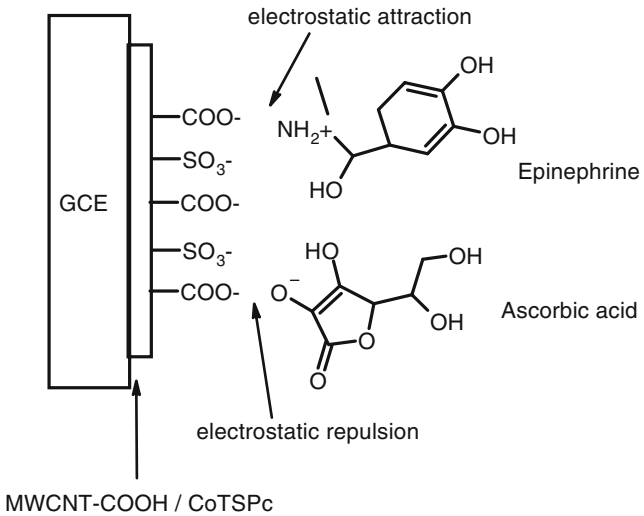

Scheme 2 Schematic representation of the interactions between the electrode surface and the species in solution at phosphate buffer pH 7.4

Figure 11a and b respectively show SWV curves obtained at different concentrations of EP (0.25 to 3.5 μA range) in the absence and presence of 1 mmol l^{-1} AA in PBS solution (pH 7.40).

AA was not detected at this concentration, which is >1,000-fold compared to that of EP concentration, and also AA presence did not significantly affect the determination of EP; the sensitivity and LoD values obtained in the absence and presence of AA are 0.0914±0.0018 A l mol^{-1} and 0.134 μmol l^{-1} and 0.0905±0.0017 A l mol^{-1} and

Table 2 Determination of epinephrine in epinephrine tartaric acid injection (1 mg ml^{-1}) solution diluted to 5×10^{-5} mol l^{-1} in phosphate buffer pH 7.4 solution

Sample	Concentration found (10^5 mol l^{-1})	Recovery (%)
1	5.05	100.6
2	5.13	102.6
3	4.97	99.4
4	4.94	98.8
5	5.21	104.1
Average % recovery	101.1±2.2	

0.140 μmol l^{-1}, respectively. This result shows that this electrode can be used to determine epinephrine in the presence of ascorbic acid in physiological pH 7.4 conditions. A notable advantage of using this electrode is the ability to completely screen out AA without the necessity to use the negatively charged nafion and at the same time no significant decrease in sensitivity for EP determination. This 'screen out' effect of AA is likely due to electrostatic repulsion between the SO_3^-/COO^- groups of both CoTSPc/MWCNT and ascorbic acid (Scheme 2), which will be negatively charged in neutral solution. The pKa_1 and pKa_2 of the enol protons of the ascorbic acid are, respectively, 4.12 and 11.6, and therefore, the first deprotonation would have occurred in pH 7.4. In addition, both GCE-MWCNT and CoTSPc-GCE electrodes only sensed EP from a mixture of EP and AA. Nano-CoPc-modified glassy carbon electrode [43] and unfunctionalized MWCNT modified basal plane pyrolytic graphite electrode [3] has been shown to sense ascorbic acid, while the non-sensing of ascorbic acid by gold nanoclusters on overoxidized polypyrrole film modified glassy carbon electrode [21] was attributed to the repulsion between the negatively charged AA at neutral solution and the carbonyl (C=O)/COO– formed during overoxidation process. It may be questioned as to why this electrostatic effect was not a major factor in the analysis using $[Fe(CN)_6]^{-3/-4}$ redox probe, which is also negatively charged. It should be noted that $[Fe(CN)_6]^{-3/-4}$ complex is a common inorganic redox probe whose redox activity is quite feasible and fast even at bare carbon electrodes. Thus, we may speculate that the impact of electrostatic effects should be less favored within the electrochemical timescale for this inorganic redox probe compared to the case of organic species like AA.

Epinephrine injection analysis

Determination of epinephrine in epinephrine tartaric acid injection solution with a specified content of EP as 1.00 mg ml^{-1} was carried out using GCE-MWCNT-CoTSPc-electrode. A 1 ml of the injection sample was diluted to 60 ml with phosphate buffer pH 7.4 to make a 5×10^{-5} mol l^{-1} solution. This solution was then analyzed using square wave voltammetry technique between −0.4 and 0.6 V at a scan rate of 100 mV s^{-1}. The assay was performed employing the standard addition method with consecutive addition of 1 ml of 10^{-4} mol l^{-1} EP standard solution in phosphate buffer. The experiment was repeated five times and the result showed a recovery between 102.6% and 98.8% (Table 2) with an average of 101.1± 2.2%, confirming that this electrode can successfully be employed for the analysis of real drug sample of epinephrine.

Conclusions

MWCNT enhances the electrochemical response of CoTSPc species. The potential for real sample applications was also proven by the ability of MWCNT-CoTSPc electrode platform to satisfactorily determine EP in the presence and absence of AA and epinephrine determination from drug samples.

Acknowledgment This work was supported by the NRF and the Universities of Pretoria and Limpopo. KIO is grateful to the South Africa's Department of Science and Technology (DST) and NRF for the Research Infrastructure Support Programme (RISP) Grants (GUN no. 65305). BOA also thanks NRF for Scarce Skill Postdoctoral Fellowship award.

References

1. Iijima S (1991) Nature 354:56–58. doi:10.1038/354056a0
2. Banks CE, Moore RR, Davies TJ, Compton RG (2004) Chem Commun (Camb) 2004:1804–1805. doi:10.1039/b406174h
3. Salimi A, Banks CE, Compton RG (2004) Analyst (Lond) 129:225–228. doi:10.1039/b315877b
4. Di-Zhao Z, Zhang W-De, Cheng H, Luo QM (2002) Talanta 58:529–534. doi:10.1016/S0039-9140(02)00318-1
5. Luo H, Shi Z, Li N, Gu Z, Zhuang Q (2001) Anal Chem 73:915–920. doi:10.1021/ac0009671
6. Musameh M, Wang J, Merkoki A, Lin Y (2002) Electrochem Commun 4:743–746. doi:10.1016/S1388-2481(02)00451-4
7. Star A, Han TR, Christophe J, Gabriel P, Bradley K, Gruner G (2003) Nano Lett 3:403–407. doi:10.1021/nl025952c
8. Leznoff CC, Lever ABP (eds) (1989–1996) Phthalocyanines: properties and applications, Vol. 1–4, VCH, New York
9. Kadish KM, Smith KM, Guilard R (eds) (2003) The porphyrin handbook, Chapters 97–122, Vol. 15–20. Academic, Boston
10. Ozoemena KI, Nyokong T (2006) In: Grimes CA, Dickey EC, Pishko MV (eds) Encyclopedia of sensors, Vol. 3. American Scientific Publishers, California, p 157 (Chapter E, and references therein)
11. Imisides MD, John R, Riley PJ, Wallace GG (1991) Electroanalysis 3:879–889. doi:10.1002/elan.1140030903
12. Siswana M, Ozoemena KI, Nyokong T (2006) Electrochim Acta 52:114–122. doi:10.1016/j.electacta.2006.03.090
13. Pillay J, Ozoemena KI, Nyokong T (2006) Electrochem Commun 8:1391–1396. doi:10.1016/j.elecom.2006.05.031
14. Pillay J, Ozoemena KI (2007) Electrochim Acta 52:3630–3640. doi:10.1016/j.electacta.2006.10.022
15. Pillay J, Ozoemena KI (2007) Chem Phys Lett 441:72–77. doi:10.1016/j.cplett.2007.04.095
16. Silva JF, Griveau S, Richard C, Zagal JH, Bedioui F (2007) Electrochem Commun 9:1629–1634. doi:10.1016/j.elecom.2007.03.008
17. Yang Z, Hu G, Chen X, Zhao J, Zhao G (2007) Colloids Surf B 54:230–235. doi:10.1016/j.colsurfb.2006.10.033
18. Gong J, Lin X (2004) Electrochim Acta 49:4351–4358. doi:10.1016/j.electacta.2004.04.024
19. Ren W, Luo HQ, Li NB (2006) Biosens Bioelectron 21:1086–1092. doi:10.1016/j.bios.2005.04.002
20. Wang L, Bai J, Huang P, Wang H, Zhang L, Zhao Y (2006) Electrochem Commun 8:1035–1040. doi:10.1016/j.elecom.2006.04.012
21. Li J, Lin X-Q (2007) Anal Chim Acta 596:222–230. doi:10.1016/j.aca.2007.05.057

22. Bai JY, Wang L, Wang HJ, Huang PF, Zhao YQ, Fan SD (2006) Mikrochim Acta 156:321–326. doi:10.1007/s00604-006-0597-7
23. Wang L, Bai J, Huang P, Wang H, Zhang L, Zhao Y (2006) Int J Electrochem Sci 153:G238–G249. doi:10.1149/1.2162452
24. He YB, Luo HQ, Li NB (2007) Instrum Sci Technol 35:163–175. doi:10.1080/10739140601126346
25. Ozoemena KI, Nkosi D, Pillay J (2008) Electrochim Acta 53:2844–2851. doi:10.1016/j.electacta.2007.10.076
26. Schenk JO, Milker E, Adam RN (1983) J Chem Educ 60:311–314
27. Banks WA (2001) Brain Res 899:209–217. doi:10.1016/S0006-8993(01)02242-9
28. Wang J, Tuzhi P, Golden T (1987) Anal Chim Acta 194:129–138. doi:10.1016/S0003-2670(00)84766-2
29. Liu J, Rinzler AG, Dai H, Hanfer JH, Bradley RK, Boul PJ et al (1998) Science 280:1253–1256. doi:10.1126/science.280.5367.1253
30. Weber JH, Busch DH (1965) Inorg Chem 4:472–475. doi:10.1021/ic50026a008
31. Lever ABP, Milaeva EL, Speier G (1993) In: Leznoff CC, Lever ABP (eds) Phthalocyanines: properties and applications, Chapter 1, Vol. 3. VCH, New York, pp 1–69
32. Tse Y-H, Janda P, Lam H, Pietro WJ, Lever ABP (1997) J Porphyrins Phthalocyanines 1:3–4 doi:10.1002/(SICI)1099-1409(199701)1:1<3::AID-JPP1>3.0.CO;2-V
33. Sabatini E, Rubinstein I (1987) J Phys Chem 91:6669–6673. doi:10.1021/j100311a022
34. Barsoukov E, Macdonald JR (2005) In: Impedance spectroscopy: theory experiment, and applications, Chapters 1–4, 2nd edn. Wiley, Hoboken
35. MacDonald DD (2006) Electrochim Acta 51:1376–1388. doi:10.1016/j.electacta.2005.02.107
36. Chen SM, Peng KT (2003) J Electroanal Chem 547:179–189. doi:10.1016/S0022-0728(03)00220-1
37. Agboola BO, Nyokong T (2007) Anal Chim Acta 587:116–123. doi:10.1016/j.aca.2007.01.031
38. Ozoemena KI, Nyokong T (2002) Electrochim Acta 47:4035–4043. doi:10.1016/S0013-4686(02)00362-6
39. Ureta-Zañartu MS, Berríos C, Pavez J, Zagal J, Gutiérrez C, Marco JF (2003) J Electroanal Chem 553:147–156. doi:10.1016/S0022-0728(03)00309-7
40. Li NB, Ren W, Luo HQ (1999) Anal Chim Acta 378:151–157. doi:10.1016/S0003-2670(98)00569-8
41. Zagal JH, Lira S, Ureta-Zanartu S (1986) J Electroanal Chem 210:95–110. doi:10.1016/0022-0728(86)90316-5
42. Collman JP, Kaplun M, Sunderland CJ, Boulatov R (2004) J Am Chem Soc 126:11166–11167. doi:10.1021/ja046768r
43. Wang K, Xu JJ, Tang KS, Chen HY (2005) Talanta 67:798–805. doi:10.1016/j.talanta.2005.04.015